Results in Materials 16 (2022) 100338

Contents lists available at ScienceDirect

Results in Materials

journal homepage: www.sciencedirect.com/journal/results-in-materials

Mesoporous boron nitride in contact with water - Chemical stability and adsorption properties

Jan Hojak [a,*,1], Tim Jähnichen [b,1], Christian Bläker [a], Christoph Pasel [a], Volker Mauer [a], Leon Rasmussen [b], Reinhard Denecke [c], Dirk Enke [b], Dieter Bathen [a,d]

[a] Chair of Thermal Process Engineering, University of Duisburg-Essen, Lotharstr. 1, 47057, Duisburg, Germany
[b] Institute of Chemical Technology, Leipzig University, Linnéstr. 3, 04103, Leipzig, Germany
[c] Wilhelm-Ostwald Institute for Physical and Theoretical Chemistry, Leipzig University, Linnéstr. 2, 04103, Leipzig, Germany
[d] Institute of Energy and Environmental Technology e.V. (IUTA), Bliersheimer Str. 58-60, 47229, Duisburg, Germany

ARTICLE INFO

Keywords:
Mesoporous turbostratic boron nitride
Air stability
Water stability
Water vapor adsorption

ABSTRACT

In the context of adsorptive water treatment, exhaust gas treatment, gas storage, or catalysis, porous boron nitride is gaining in scientific attention due to its versatile properties. The material is above all characterized by its high chemical and thermal stability. However, it has recently been shown that porous boron nitride is highly water-susceptible, which severely limits its application in non-inert atmospheres. So far, solely the influence of chemical composition on water stability has been investigated in literature. In the present work, the influence of different pore sizes is considered. Two different boron nitrides, a mesoporous and a micro-mesoporous one, are investigated with regard to their stability in air, water vapor, and liquid water for multiple weeks. Using different analytical methods, it can be shown that the stability of porous boron nitride strongly depends on pore size and structure. We demonstrate that the mesoporous boron nitride synthesized in this work has much higher water stability than micro-mesoporous boron nitrides. The mesoporous material showed minor to no changes in its chemical structure and isothermal shape when exposed to water vapor and air. We suggest that a higher amount of crystalline hexagonal boron nitride leads to increased stability. This conclusion opens pathways to improve the water stability of porous boron nitride in order to make it suitable for non-inert gas phase adsorption applications.

1. Introduction

New materials for energy storage [1], catalysis [2,3], or adsorption [4,5] are tested to improve industrial processes. One of the materials with promising properties in these fields is hexagonal boron nitride (h-BN) [6–10]. Hexagonal BN is well known for its large bandgap, electric insulation, high thermal conductivity, chemical resistance, and thermal stability [11]. Despite its special properties, its utilization is still limited by low porosity and specific surface area. To synthesize a more porous BN material, the synthesis of turbostratic boron nitride (t-BN) was studied extensively over the last years. Contrary to h-BN the material shows high specific surface areas up to 2078 $m^2\ g^{-1}$ [12]. The higher porosity of t-BN is driven by a twisting of BN layers between one another, which forms defects in the structure in the dimension of micropores [13]. Due to its higher porosity t-BN can be used for catalysis [14], gas storage [15], or water treatment [16]. To achieve the highest efficiency for those applications, the synthesis of highly porous BN is currently being pursued and its application investigated. However, the synthesis of porous BN is accompanied by a loss of crystallinity and thus stability of the material. In previous works it was shown that amorphous BN (a-BN) reacts with water at room temperature [17]. A recent work of Shankar et al. [18] showed that porous BN is chemically unstable to water, limiting its application in various areas. They investigated the stability of a high specific surface area BN (1666 $m^2\ g^{-1}$) towards liquid and gaseous water. It was shown that after water exposure for 24 h the specific surface area of the material was reduced to 51 $m^2\ g^{-1}$ in liquid water and below 10 $m^2\ g^{-1}$ in vapor. In addition, they observed an increase in crystallinity after water exposure which is explained by the decomposition of a-BN or t-BN while stable h-BN remained. Furthermore, their work indicates that porous BN materials with a low specific

* Corresponding author.
E-mail address: jan.hojak@uni-due.de (J. Hojak).
[1] J. H. and T. J. contributed equally to this paper.

https://doi.org/10.1016/j.rinma.2022.100338
Received 15 July 2022; Received in revised form 26 September 2022; Accepted 19 October 2022
Available online 20 October 2022

surface area react with water and start to decompose. Similar results were reported later on [19]. For long storing durations under atmospheric conditions Alkoy et al. [20] were able to show that turbostratic boron nitride decomposes into an ammonium borate compound. To summarize, knowledge about the influence of different synthesis parameters on the chemical stability and resulting properties of porous BN is still scarce and further research is necessary.

In this work, we utilized a pre-heating method previously described by Jähnichen et al. [21]. This method yields mainly mesoporous t-BN which exhibits much higher water stability than previously reported microporous t-BN materials. A template-free synthesis was used. Boron and nitrogen precursors are homogeneously mixed, and then reacted in an inert gas atmosphere (N_2, NH_3, Ar) to form BN. The properties of the product are influenced by choice of precursors, their ratio, and used synthesis parameters. Especially the nitrogen precursors affect the pores in the product significantly. While melamine-based BN is primarily microporous, nitrogen precursors such as biuret or urea lead to the formation of micro- and mesopores [22]. Using urea as a nitrogen precursor and controlling its decomposition by adding a pre-heating step we were able to synthesize a highly mesoporous BN material with nearly no microporosity and high crystallinity [21]. The chemical durability of the synthesized mesoporous BN and a micro-mesoporous BN reference sample are compared regarding their stability in different environments: air, gaseous water (referred to as vapor), and liquid water (referred to as water). To observe changes within the properties of the different BN materials during exposure, the samples were characterized by X-ray diffraction (XRD), X-ray photoelectron spectroscopy (XPS), scanning electron microscopy (SEM), mercury intrusion, attenuated total reflection - infrared spectroscopy (ATR-IR), thermogravimetry (TG), and nitrogen sorption.

2. Experimental

2.1. Synthesis of mesoporous t-BN

For the synthesis of mesoporous t-BN urea (Alfa Aesar, 98+%) and boric acid (VWR Chemicals, 99+%) were used in a molar ratio of boric acid to urea 1:3. Both precursors were homogeneously ground in a ball mill (PM 100, Retsch, 450) for 5 min (450 rpm). After that, the homogeneous precursor mixture was transferred to an alumina combustion boat crucible and heated in a tube furnace (ROC 50/610/14, Thermconcept). Two heating levels were chosen: 200 °C for 2 h followed by 1300 °C for 4 h with a heating rate of 5 K min^{-1}. The synthesis was performed in a nitrogen atmosphere (purity 5.0) at a constant flow rate of 80 l h^{-1}. After the synthesis, approximately 0.8 g of a flake-like white BN were obtained. The synthesis was performed multiple times to gain approximately 12.5 g of the sample which was homogenized to inhibit reproduction deviations. In the following, the mesoporous sample is referred to as BN-meso.

2.2. Synthesis of the micro-mesoporous t-BN reference sample

The synthesis of the micro-mesoporous t-BN reference sample was carried out similar to the mesoporous sample. Boric acid and urea were also used as precursors in a molar ratio of 1:3. The precursors were ground as explained previously. The mixture was transferred to an alumina combustion boat crucible and heated in one step to 1300 °C (5 K min^{-1}) in a tube furnace. The temperature was maintained for 4 h. For the synthesis, a nitrogen flow of 150 l h^{-1} was applied. For the micro-mesoporous material, approximately 3 g of the sample (0.8 g each approach) were synthesized and homogenized. The micro-mesoporous reference sample is referred to as BN-ref in this work.

2.3. Investigation of the air stability

The air stability of the samples has been investigated for up to 12 weeks. Each sample was transferred to a 50 ml polypropylene (PP) beaker, which was stored at room temperature in a fuming hood (humidity ~ 30%). After 1 week, 2 weeks, 4 weeks, and 12 weeks approximately 0.2 g of each sample were removed for analysis.

2.4. Investigation of the water vapor stability

Water vapor adsorption was investigated in an autosorb iQ3 (Quantachrome Instruments). The isotherms were measured volumetrically at 25 °C in a relative pressure range of $0.0 < p\,p_0^{-1} < 0.9$. Before the measurements, the samples were outgassed for at least 4 h up to 6 h under vacuum at 150 °C. Outgassing was considered sufficient once the pressure increase was less than 25 mtorr min^{-1}.

2.5. Investigation of the water stability

To observe the water stability approximately 0.16 g of the material was transferred in a 50 ml PP beaker at room temperature. 40 ml of deionized water and a stirrer were added. After closing the beaker, the mixture was stirred at 500 rpm. For each time point (0.5 h, 6 h, 48 h, 1 week, 2 weeks, 4 weeks) a separate solution was made. After the assigned time passed, the stirrer was removed and the mixture was aspirated through a G4 glass frit. In the end, the filtrate was washed with 50 ml deionized water and then dried in an oven at 80 °C for 24 h (DRY-Line, VWR).

2.6. Material characterization

The XRD analysis was performed with the device STOE STADIP (STOE & Cie GmbH) equipped with a Mythen 1 K detector (DECTRIS). As radiation Cu Kα (40 kV, 40 mA) was used. A step-width of 0.2 °2θ s^{-1} was applied. The spectra were evaluated by Match! (Version 3.3.0, Crystalimpact).

ATR-IR measurements were carried out with an Alpha II FT-IR spectrometer from Bruker. A platinum ATR module with a diamond crystal was used. Prior to the analysis approximately 5–10 mg powdered sample were put on the crystal. The measuring was performed between 500 and 4000 cm^{-1} with a resolution of 4 cm^{-1}. Each scan was replied 20 times.

A VG ESCALAB 220i-XL measurement device (Thermo Scientific) with an Al-anode (12 kV, 20 mA, 240 W) was used to perform XPS analysis. As radiation Al Kα was emitted. The measurement was performed in a vacuum (10^{-8} mbar) in the electron binding energy range of - 5 to 1205 eV. A step size of 0.5 eV (survey scan) and 0.1 eV (detail spectra) at pass energy of 50 eV were used. Every scan was repeated 4 times. Before analysis, the samples have been mounted on conductive carbon tape. Unifit 2022 [23] was used to evaluate the spectra. Peaks are fitted by Voigt profiles. Excitation satellites and a suitable background have been subtracted.

SEM was performed with a Nova NanoLab200 from FEI Company equipped with an Everhart-Thornley-Detector. A measurement voltage of 10–15 kV and an electron gun distance of 5 mm were used. Before the analysis, the samples were steamed with gold.

The characterization of the pore system of BN materials followed those of activated carbons [24].

The porosity of the macropores between 50 and 10000 nm was investigated by mercury intrusion with the devices Pascal 140 and Pascal 440 by Porotec. After weighing approximately 50–100 mg of the sample in a dilatometer, the dilatometer was transferred to the Pascal 140, evacuated to 0.2 mbar, and then filled with mercury. The intrusion measurement up to 400 MPa was carried out in the Pascal 440 at room temperature. The mercury contact angle was set to 140° and surface tension to 0.48 N m^{-1}.

An autosorb iQ3 (Quantachrome Instruments) was used to measure nitrogen sorption isotherms at 77 K. The samples were outgassed in the same manner as for the water adsorption measurements. BET (Brunauer-

Emmet-Teller) surface areas [25] were determined according to DIN ISO 9277 [26], mesoporous surface areas according to DIN 66134 [27], utilizing the method of Barrett, Joyner, and Halenda [28,29], and microporous surface areas according to DIN 66135 [30] with the t-method by Lippens and de Boer [31]. In the latter, the subtraction of the external surface area from the BET surface area resulted in the surface area of the micropores. Pore size distributions were determined using QSDFT for the adsorption branch of nitrogen sorption at 77 K on carbon with slit and cylindrical pores.

3. Results and discussion

3.1. Comparison of the sample properties

To evaluate the stability of BN-meso and BN-ref their properties have to be compared. For that, XRD, SEM, nitrogen sorption, and mercury intrusion were used.

The crystallinity of the materials was investigated by XRD. As depicted in Fig. 1 the diffractograms display three reflexes at $2\theta = 26°$, $2\theta = 43°$ and $2\theta = 76°$ which can be assigned to the (002), (10), and (110) planes of h-BN respectively [32,33]. Nevertheless, the reflex width of both materials is broad which implies a turbostratic structure. By comparing the diffractogram of BN-meso to the reference sample BN-ref a smaller reflex width and signal-to-noise ratio are observed for BN-meso. This suggests, that BN-meso has higher crystallinity than the reference sample. It can be assumed that the higher crystallinity is due to a less disordered crystal structure which is caused by a lower microporosity.

To better understand pore structure and porosity within the two samples, nitrogen sorption and mercury intrusion were performed. Nitrogen sorption at 77 K was used to observe changes within micro- and mesopores, whilst macropores were analyzed by mercury intrusion. The nitrogen adsorption isotherms are depicted in Fig. 2 (a). Both materials show Type IV(a) behavior with H5 hysteresis loops, according to the IUPAC classifications [34]. After an initial uptake of nitrogen, the isotherm of BN-meso displays a sharp knee followed by a linear rise up to $p\ p_0^{-1} = 0.6$. This indicates a mainly mesoporous pore structure with only a small amount of micropores and no significant overlap between mono- and multilayer adsorption. At higher relative pressures capillary condensation takes place and the pore system is filled with nitrogen until an inflection point is reached. The desorption branch does not descend until $p\ p_0^{-1} < 0.9$ and follows the trend of the adsorption branch. A sharp step-down of the desorption branch takes place at $p\ p_0^{-1} = 0.5$. The shape of the hysteresis loop is typically associated with both open and partially blocked mesopores.

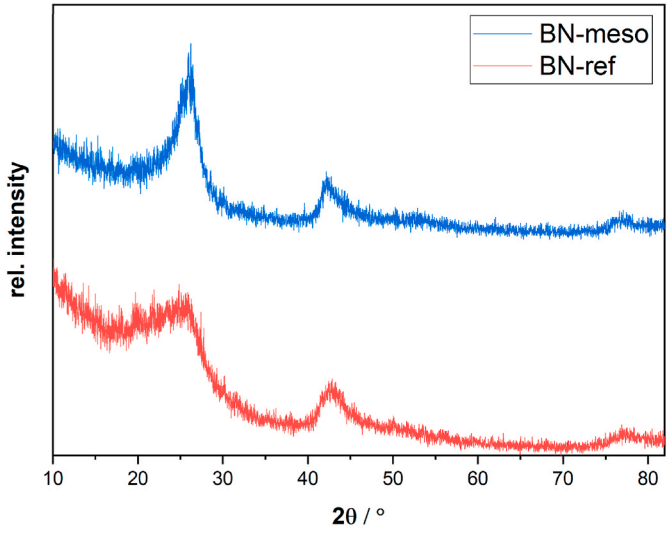

Fig. 1. XRD patterns of BN-meso and BN-ref.

The shape of the isotherm of BN-ref is similar to BN-meso. The main differences can be found in the higher nitrogen adsorption capacity and the steeper increase at low relative pressures for BN-ref. The shapes of the hysteresis loops are similar for both materials, which indicates comparable mesopore volumes. Thus, similar mesoporosities and different microporosities can be expected. BET surface areas and pore volumes for both materials are given in Table 2 (BN-ref) and Table 3 (BN-meso) below. As deduced from the nitrogen sorption isotherms, BN-meso has a smaller BET surface area (214 $m^2\ g^{-1}$) and total pore volume (0.51 $cm^3\ g^{-1}$) than BN-ref (567 $m^2\ g^{-1}$, 0.66 $cm^3\ g^{-1}$). The most significant difference can be found in the micropore surface area, with BN-meso having a low micropore surface area of 55 $m^2\ g^{-1}$, whilst BN-ref features a micropore surface area of 423 $m^2\ g^{-1}$ that is about eight times larger. We assume, that the sample shows a higher microporosity due to its lower crystallinity and thus higher turbostratic or amorphous proportion. This leads to more twists within the BN planes, creating gaps in the size of micropores. Since larger mesopores are formed mainly by foaming processes during precursor decomposition, they are less affected by changes in crystallinity.

Larger pores of the materials were investigated by mercury intrusion. The pore width distributions of mesopores above 10 nm and macropores up to ~13000 nm are shown in Fig. 2 (b). Both samples have a similar pore width distribution, however, BN-ref depicts a slightly higher cumulative pore volume and porosity than BN-meso (Table S1). We assume that the lower pore volume and porosity of BN-meso occur due to the preheating at 200 °C and thus less foaming at higher temperatures.

To observe morphology and structure of the material SEM was applied. As shown in Fig. 3 (a) the sample BN-ref depicts a non-ordered flake-like morphology, that is typically reported in literature for urea-based BN materials [35]. BN-meso has a different type of morphology. In Fig. 3 (b) a smooth surface is observed, which is imbued by tubular cracks. The surface is formed by multiple stacked flakes that partially show up. We assume that the changes in the morphology arise because of the introduced pre-heating step which enables formation of larger urea decomposition intermediates.

In summary, pre-heating at 200 °C BN-meso yields a more crystalline material with 8 times lower microporosity. Hence, two materials were synthesized: BN-ref is a micro-mesoporous material with lower crystallinity, and BN-meso is a mainly mesoporous material with higher crystallinity. Comparing both materials by nitrogen sorption and mercury intrusion, only minor changes are observed in the meso- and macropore range. Therefore, the samples are suitable to investigate stability of different pore types in t-BN (e. g. micro- and mesopores) on vapor and water.

3.2. Stability to air and vapor

To store or to use t-BN in the presence of air, the material must be resistant to oxidation and inert to vapor. While BN is generally highly resistant to oxidation up to 700–800 °C (Fig. S1), it is well known that it has low stability against water due to its rapid decomposition to boron oxide and ammonia [18,36]. To observe whether the mesoporous BN material shows higher air stability than other t-BN materials its long-term stability for up to 12 weeks was investigated and compared to the sample BN-ref. All samples were analyzed by nitrogen sorption. Furthermore, XPS, XRD, and IR were applied to detect changes within the chemical structure of the materials.

The B 1s XPS spectra are shown in Fig. 4. In all spectra, two main contributions and a satellite are used. The peak at a binding energy of ~193.1 eV is assigned to B–O and the peak at ~191.1 eV to B–N [37]. The B–O signal arises due to initially unreacted boron oxide or due to boron oxide later formed by a reaction with water vapor. The shake-up satellite can be attributed to B–N double bonds within hexagonal domains [38]. To evaluate the air stability of the materials their B–N to B–O ratio was calculated from the B 1s spectra. An overview of the

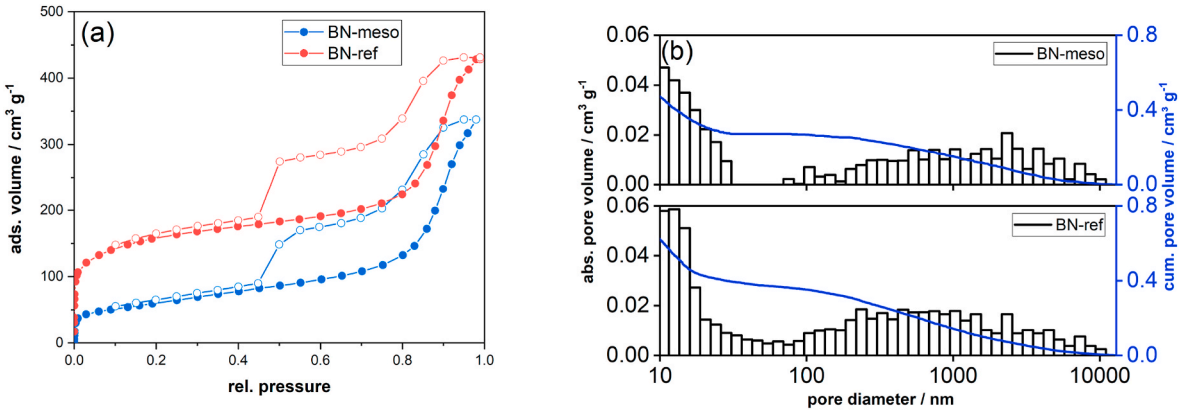

Fig. 2. (a) Nitrogen adsorption isotherms at 77 K and (b) mercury intrusion results of BN-meso and BN-ref.

Table 1
B–N to B–O ratio after the synthesis, 4 weeks and 12 weeks calculated by XPS (B 1s).

Exposure time	BN-ref	BN-meso
new	97:3	96:4
4 weeks	91:9	96:4
12 weeks	88:12	97:3

Table 2
BET surface areas and pore volumes of BN-ref after the synthesis, water-vapor adsorption (WVA) and air exposure.

Exposure time	BET surface area/$m^2\ g^{-1}$	micropore surface area/$m^2\ g^{-1}$	micropore volume/$cm^3\ g^{-1}$	total pore volume/$cm^3\ g^{-1}$
new	567	423	0.19	0.66
Water-vapor adsorption				
after WVA	131	30	0.01	0.38
Air exposure				
1 week	441	309	0.14	0.57
2 weeks	326	174	0.08	0.57
4 weeks	206	80	0.04	0.44
12 weeks	132	26	0.01	0.39

Table 3
BET surface areas and pore volumes of BN-meso after the synthesis, water-vapor adsorption (WVA), and air exposure.

Exposure time	BET surface area/$m^2\ g^{-1}$	micropore surface area/$m^2\ g^{-1}$	micropore volume/$cm^3\ g^{-1}$	total pore volume/$cm^3\ g^{-1}$
new	214	55	0.03	0.51
Water-vapor adsorption				
after WVA	211	24	0.01	0.52
Air exposure				
1 week	191	15	0.01	0.50
2 weeks	170	14	0.01	0.48
4 weeks	167	<10	<0.01	0.48
12 weeks	146	<10	<0.01	0.46

calculated ratios is given in Table 1. By comparing the starting materials, it has to be noted that both depict a similar B–O content within the error bars of the method, and therefore, differences in the stability due to different initial oxygen impurities can be excluded. For the sample BN-ref, it can be seen that the ratio of B–N to B–O is changing within 12 weeks. Directly after the synthesis, the sample shows a high purity with ~3% of B–O-impurities present. After 4 weeks the amount of B–O increased to ~9%, increasing further to ~12% after 12 weeks. To evaluate the influence of air on the decomposition of the material, the same sample has been stored additionally in vacuum atmosphere (Fig. S2). Thereby no increase in the B–N to B–O ratio were observed. Hence, the observed change must result from a reaction with ambient air whereby a B–O species is formed. To depict the ongoing reaction XRD and IR analysis were carried out on the 12-week-old sample. In the XRD measurement, no new reflexes indicating a B–O species could be detected (Fig. S4 (a)). Nevertheless, changes in the reflex width of the sample can be seen, which suggests an ongoing reaction of the material. This assumption is further supported by the results of IR spectroscopy. As shown in Fig. 5 (a) before air exposure BN-ref shows two distinct bands at ~ 1360 cm^{-1} and ~800 cm^{-1}. The band at ~1360 cm^{-1} can be attributed to an in-plane transverse B–N stretching vibration and the band at ~800 cm^{-1} to an out-of-plane B–N–B bending vibration. Both bands indicate a BN material with a low amount of impurities. On the other hand, after air exposure, a shoulder at the B–N band [39] and a broad band with a peak at ~ 3200 cm^{-1} and a shoulder at ~ 3400 cm^{-1} can be observed. The significant peak of this band at ~3200 cm^{-1} can be assigned to NH_2 groups [40] whilst the shoulder at ~ 3400 cm^{-1} can be attributed to a formation of O–H and N–H groups, due to an ongoing reaction with water from air. Hereby a formation of boron oxynitride is assumed. This assumption is supported by the observed shoulder at ~1000 cm^{-1} which is attributed to a B–O band [41]. Based on these results, the formation of an amorphous B–O species detected by XPS can be verified.

The B–O formation affects the porosity of the material as well. In Fig. 5 (c) nitrogen sorption isotherms of the sample BN-ref after different air exposure times are shown. As depicted, with prolonged exposure, the adsorbed nitrogen volume, and thus, the total pore volume decreases, indicating a reaction on the surface of the material that either blocks or narrows the pores until they are no longer accessible. Since there are no observable changes in the hysteresis loop with prolonged air exposure, it can be assumed that the proposed reaction blocks primarily micropores by forming a sterically larger B–O species. This assumption is further supported by the BET and micropore surface area results. As shown in Table 2, within 12 weeks the BET surface area decreases from 567 $m^2\ g^{-1}$ to 132 $m^2\ g^{-1}$ and the micropore surface area from 423 $m^2\ g^{-1}$ to 26 $m^2\ g^{-1}$. By comparing these losses, it can be seen, that the loss in BET surface area is primarily driven by a loss of micropores. Based on these results it can be assumed that the sample BN-ref is not stable to ambient air and hence its usage for non-inert applications has to be reviewed carefully. Considering the high oxidation stability, it is assumed that water vapor is the main antagonist to material stability.

In comparison to BN-ref, the mesoporous sample BN-meso shows a different behavior regarding its air stability as depicted by XPS, XRD, and nitrogen sorption. In XPS measurements the sample BN-meso shows initially ~4% of B–O impurities (Table 1). Contrary to the micro-mesoporous sample no changes in the B–N to B–O ratio can be observed within 12 weeks which implies no chemical reaction with

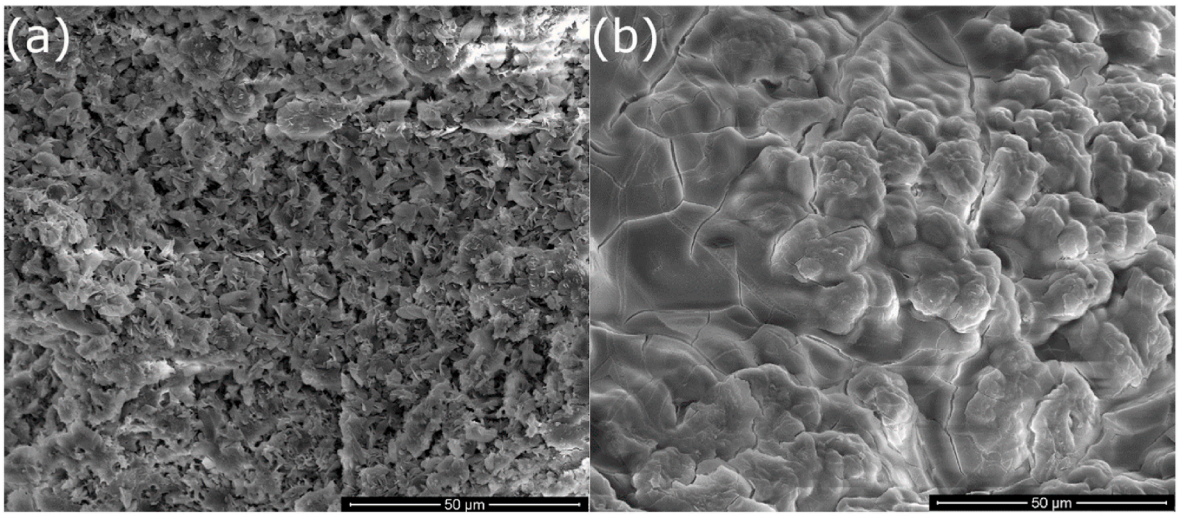

Fig. 3. SEM images of (a) BN-ref and (b) BN-meso. The image scale is 50 µm.

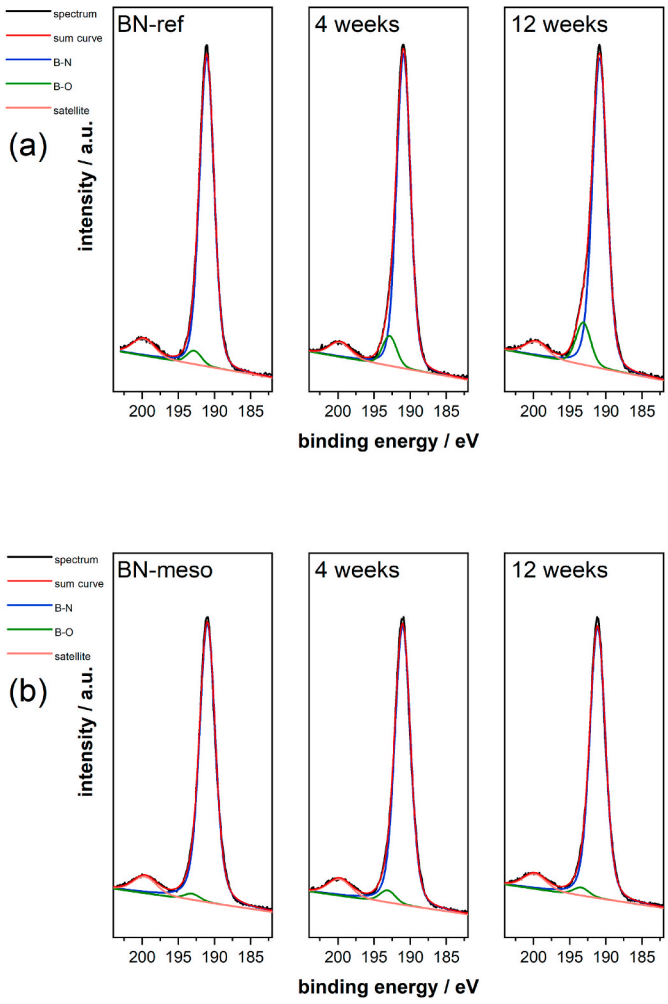

Fig. 4. Normalized B 1s XPS measurements of (a) BN-ref and (b) BN-meso. Investigation of the air stability for up to 12 weeks.

vapor in the air (Fig. S3). This assumption is supported by XRD and IR measurements. As shown in Fig. S4 (b) in the XRD spectra no additional reflexes and no significant changes in the reflex width are depicted within 12 weeks. Nevertheless, a reduction of the signal-to-noise ratio can be observed. In the IR spectra (Fig. 5 (b)) a slight increase in the B–OH band at 3400 cm^{-1} is depicted which probably arises due to water adsorbed from air. The NH_2 peak described before also increases slightly. All other bands (B–N and B–N–B) do not show any significant changes which indicates an air stable material as well.

In Fig. 5 (d) the nitrogen sorption isotherms for the sample BN-meso are presented. Only small changes in the adsorbed volume can be observed up to 8 weeks of exposure. After that, a slight decrease in the pore volume is detected. The calculated pore volumes and BET surface areas are given in Table 3. After 12 weeks of exposure, the BET surface area of the initial sample (214 $m^2\ g^{-1}$) is reduced to 146 $m^2\ g^{-1}$. Considering the calculated micropore surface area most of the changes in pore structure seem to arise due to a reduction of micropores. The micropore surface area decreases from initially 55 $m^2\ g^{-1}$ to <10 $m^2\ g^{-1}$ after 4 weeks. It is evident that the decrease in BET surface area is solely due to the decrease in micropore surface area. Hence, it can be assumed that in BN micropores are labile to vapor and mesopores have a higher resistance. We expect that a reaction with water vapor from the air takes place at the pore surface, blocking micropores and narrowing mesopores with increasing length of time (Fig. S6). Due to the higher crystallinity and lower microporosity, this reaction is less pronounced in BN-meso, which is why no changes in chemical composition were detectable by XRD, XPS, or IR.

It could thus be shown that the newly synthesized mesoporous sample exhibits much higher air stability than conventional micro-mesoporous t-BN. Not only the original oxygen content of the material, as reported by Shankar et al. [18], seems to influence the stability but also the pore type present. We were able to demonstrate that a reaction with water from air and thus a reduction of the surface area and pore volume in BN occurs less pronounced in mesopores.

To verify in detail how stable the sample is towards a pure vapor atmosphere, water vapor adsorption (WVA) measurements on BN-meso and BN-ref were compared. The water vapor isotherms of both materials are depicted in Fig. 6. Up to $p\ p_0^{-1} = 0.25$, both isotherms show a similar shape with a comparable uptake of water. The steep uptake at low partial pressures indicates a hydrophilic surface as already discussed in a previous work by Shankar et al. [18]. The hydrophilic properties might be attributed to oxygen-containing defects within the pores. The similar isotherm shapes correspond to the similar oxygen content of BN-meso and BN-ref. At higher relative pressures the shape of the isotherms and the adsorption capacities differ significantly. Whilst BN-meso can roughly be classified to be Type IV(a) with an H5 hysteresis loop, BN-ref displays a highly unusual behavior. In the range of $0.3 < p\ p_0^{-1} < 0.6$ the adsorption branch follows a steep linear increase. We assume that a

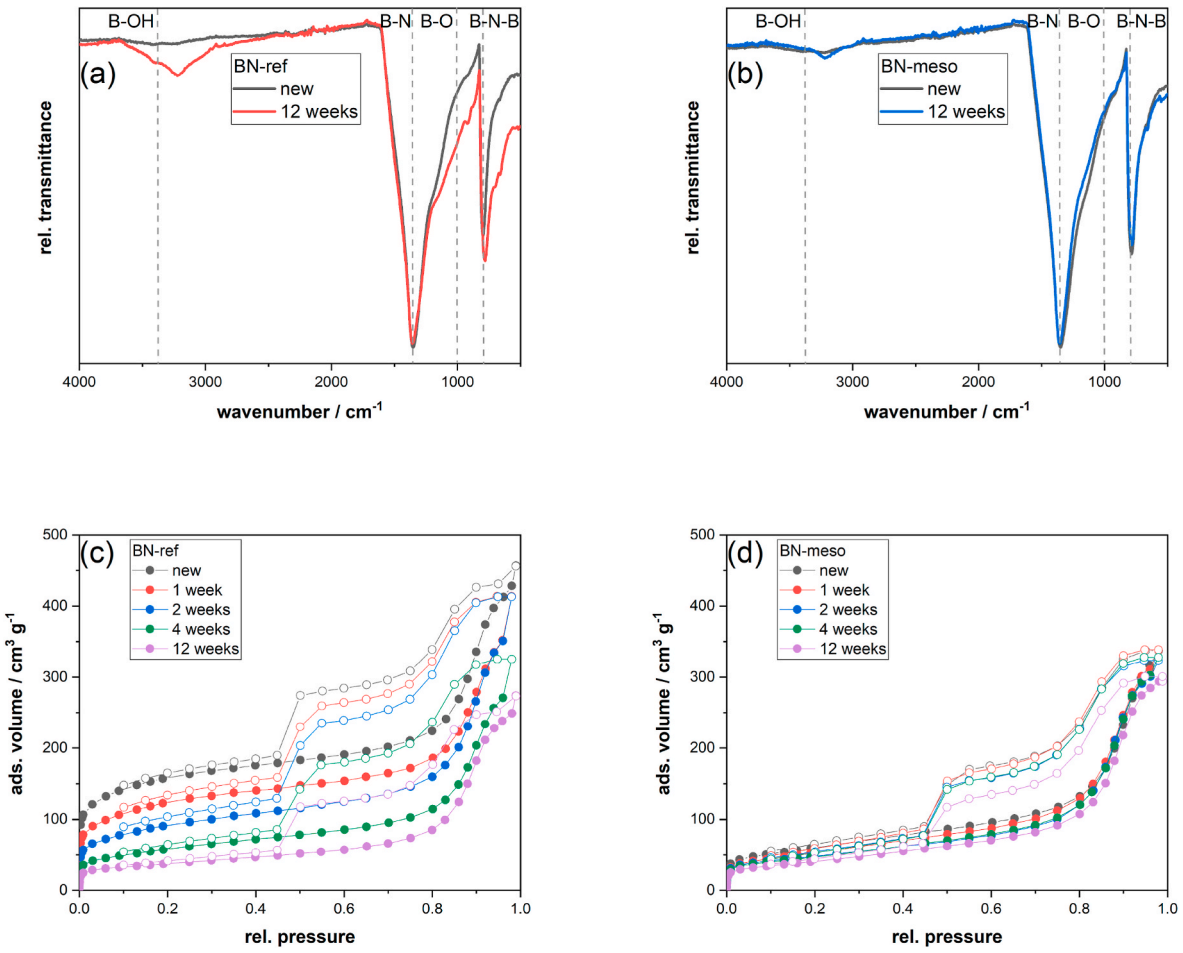

Fig. 5. IR spectra of (a) BN-ref and (b) BN-meso and nitrogen sorption isotherms at 77 K of (c) BN-ref and (d) BN-meso after up to 12 weeks of air exposure.

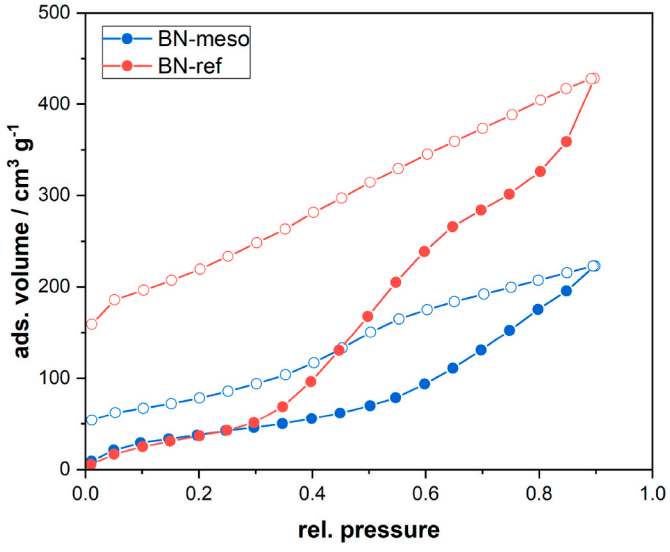

Fig. 6. Water vapor adsorption isotherms of BN-meso and BN-ref at 298 K.

chemical reaction with water takes place after a certain amount of water is adsorbed on the surface of BN-ref. This chemisorptive loading increases the amount adsorbed and at the same time reduces the pore volume significantly (Table 2). Once this reaction is completed (at $p\,p_0^{-1} > 0.6$) physisorption continues until the pore system is saturated. We hypothesize that the amount of chemisorbed vapor depends on the amount of micropores in the material. Thus, mesoporous BN adsorbs less water and therefore reacts less strongly. For both samples, the hysteresis loops are not closed. However, the gap for BN-ref is at least four times that of BN-meso. In general, an open hysteresis loop indicates non-reversibility of the adsorption process and thus chemisorption. Hence, both materials seem to chemisorb vapor. Based on these results, it can be concluded that BN-ref and BN-meso react with water. Nevertheless, the mesoporous material shows much higher stability towards vapor compared to BN-ref and previously reported high surface area BNs [18].

To determine the influence of vapor adsorption on the pore structure, the samples were characterized by nitrogen sorption. Fig. 7 depicts the nitrogen isotherms before and after the contact with water vapor. BN-ref (Fig. 7 (a)) shows a significant change in the shape of the isotherm after water vapor adsorption. In addition, the adsorbed nitrogen volume, total pore volume, and BET surface area are reduced significantly. The reduction in surface area can again be attributed to a loss of micropores (Table 2). The pore size distributions of BN-ref before and after water vapor adsorption underline this suggestion (Fig. 7 (b)). After vapor adsorption, almost all micropores and a small amount of mesopores are lost. By comparing the results to the material stored in ambient air, we observe that the pore structure is very similar to the one after 12 weeks in air, supporting the theory of water as the main antagonist to material stability.

Identical measurements were carried out for BN-meso (Fig. 7 (c)). Hereby no significant changes in the isotherm can be observed. It seems like water, which reacts with the surface, is not relevant to water adsorption and some, if not all, of the remaining water was removed during the pre-measurement conditioning. However, when looking at

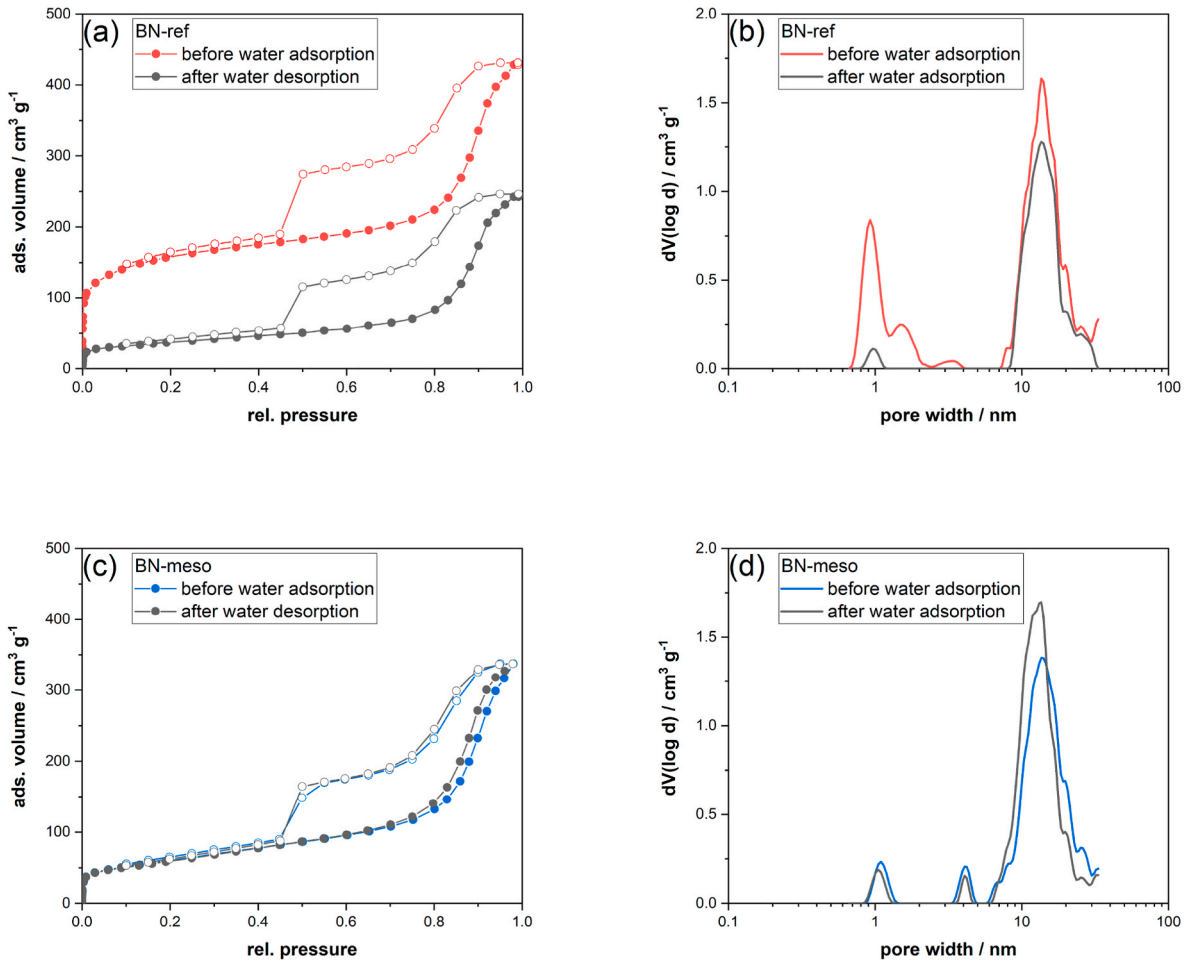

Fig. 7. Nitrogen adsorption at 77 K (a), (c) and pore size distribution (b), (d) of BN-ref and BN-meso before and after water vapor adsorption.

the pore distribution of the BN-meso sample (Fig. 7 (d)), changes in the mesopore distribution are visible. Compared to the initial material, a higher amount of mesopores between ~8 and ~20 nm is more narrowly distributed. A similar pore size distribution is received after 2 weeks of air storage. As already mentioned we assume that the changes in pore system are driven by a B–O formation on the pore surface, whereby micropores are blocked and mesopores are narrowed.

In Table 2 (BN-ref) and Table 3 (BN-meso) the BET surface areas, as well as the pore volumes of the materials prior to and after water vapor adsorption, are given. As discussed above, the porosity and BET surface area of BN-meso remains nearly unchanged, with only a small loss in micropore surface area and an insignificantly higher total pore volume. Compared to that, BN-ref loses more than 75% of its BET surface area, almost all of its microporous surface area, and approximately 50% of the total pore volume due to water vapor adsorption. Hence, we expect a similar reaction between the vapor and the more microporous BN-ref as already proposed for air exposure. We assume that the reaction products formed either block access to micropores or clog them completely making them inaccessible to gases. Considering that water vapor is present in almost all technical adsorption applications, the more microporous BN-ref has to be improved further before usage in gas phase adsorption. The results of water vapor adsorption confirm our suggestion that micropores in BN significantly reduce stability of the material, while mesopores exhibit very high vapor stability.

3.3. Stability to liquid water

Both materials are analyzed by nitrogen sorption and XRD after exposure to liquid water for 1, 2, and 4 weeks. The water stability of the sample BN-meso was additionally investigated by nitrogen sorption after 0.5, 6, and 48 h to observe changes within the shape of the isotherm and BET surface area. The mass loss after the water exposure is shown in Table S2. It can be seen that the mass loss increases slightly for BN-meso with increasing water exposure time. The mass loss remains nearly constant for BN-ref. After 4 weeks of exposure time, both materials loose roughly a third of their mass (BN-ref ~ 40%, BN-meso ~ 30%).

At first, properties of the reference sample BN-ref are discussed. In Fig. 8 (a) the XRD spectra of BN-ref after different water exposure times are shown. As depicted in the diffractograms the reflex width of the main BN reflex at $2\theta = 26°$ is decreasing after 1 week of exposure which indicates an increase in crystallinity. The higher crystallinity is attributed to the decomposition of amorphous and turbostratic BN to boric acid and ammonia in the presence of water [18,36]. Since these decomposition products dissolve in water just highly crystalline BN remains.

The decomposition of amorphous and turbostratic BN affects the porosity of the sample as well which was investigated by nitrogen sorption. As shown in Fig. 9 (a) an increased contact time reduces the amount of adsorbed nitrogen and thus the porosity of the material. The calculated surface areas and pore volumes are given in Table 4. The pore size distributions are presented in Fig. S9. Considering the results given above, initially the amorphous and turbostratic BN decomposes resulting in a significant loss of pore volume and BET surface area. After 1 week of water exposure, BET surface area and pore volume of the material are halved. After 2 weeks a slight increase of the BET surface area can be observed, whilst the pore volume decreases further. We propose

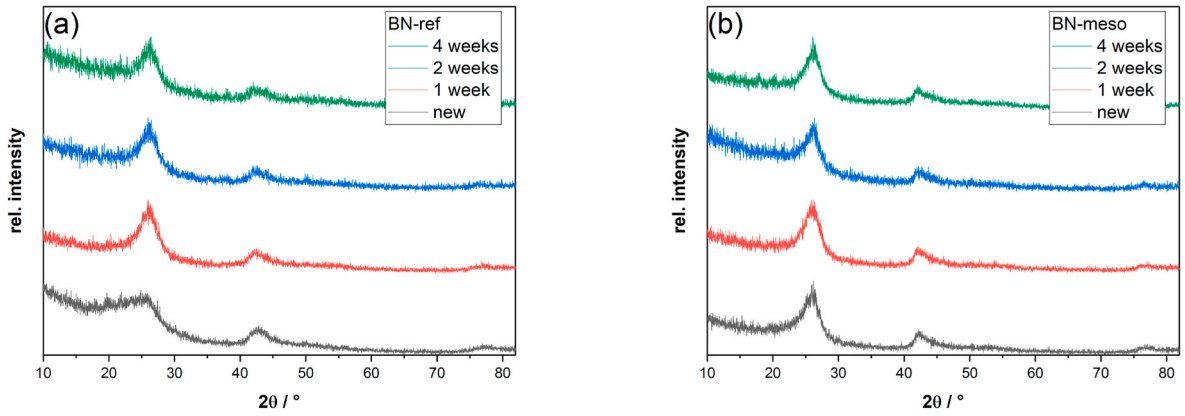

Fig. 8. XRD patterns of (a) BN-ref and (b) BN-meso after exposure to water.

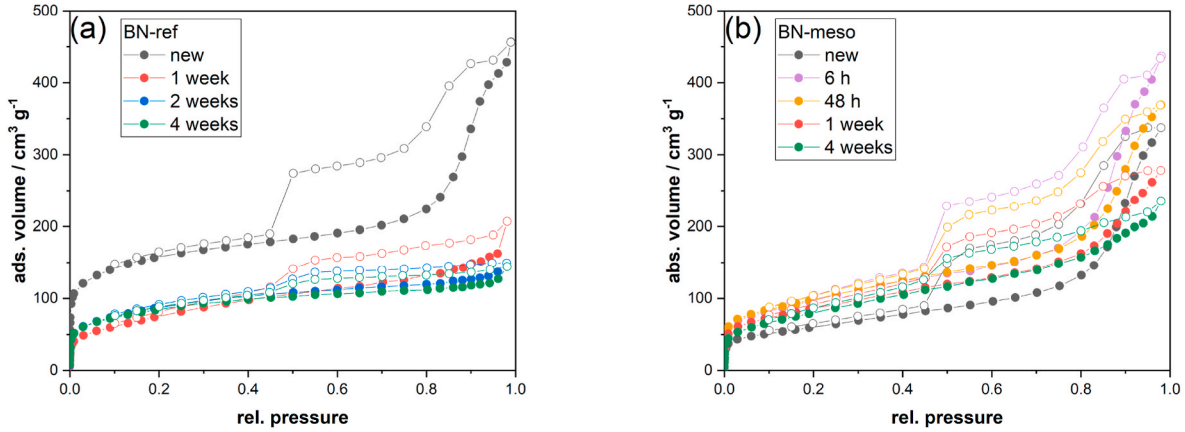

Fig. 9. Nitrogen adsorption isotherms at 77 K of (a) BN-ref and (b) BN-meso after storage in liquid water.

Table 4
BET surface areas and pore volumes of BN-ref and BN-meso after water exposure.

Water exposure time	BET surface area/m^2 g^{-1}	micropore surface area/ m^2 g^{-1}	micropore volume/cm^3 g^{-1}	total pore volume/cm^3 g^{-1}
BN-ref				
1 week	276	170	0.10	0.32
2 weeks	310	260	0.14	0.23
4 weeks	300	258	0.13	0.22
BN-meso				
0.5 h	343	84	0.04	0.66
6 h	349	158	0.08	0.68
48 h	350	164	0.09	0.57
1 week	307	134	0.07	0.43
2 weeks	287	137	0.07	0.38
4 weeks	292	128	0.08	0.36

that reaction products narrow the size of some mesopores to the size of micropores. By increasing the exposure time to 4 weeks no further changes can be observed. Correspondingly to the weight loss described above, BN-ref decomposes strongly within 1 week and continues to decompose slowly over time. Therefore, applications in water have to be considered carefully.

Compared to the micro-mesoporous material, BN-meso exhibits no significant changes in the XRD spectra (Fig. 7 (b)), regardless of the exposure time, which implies higher water stability. Nevertheless, considering the nitrogen sorption results a different trend is displayed. As shown in Fig. 9 (b) after up to 6 h of water exposure an increase in the adsorbed nitrogen volume can be observed. Thereby the total pore volume and BET surface area increase (Table 4). We propose that this initial increase results from a dissolution of unreacted boron oxide which leads to an opening of blocked pores [18]. By prolonging the exposure time further, a decrease in the adsorbed nitrogen volume can be observed. Thus, the total pore volume (after 48 h) declines with increasing exposure time. In comparison to that, the decline in BET surface area is less distinct and remains partially constant after 1 week (~300 m^2 g^{-1}). In addition, a change in the hysteresis loop can be observed. Whilst the initial material has a similar shape to H5, with prolonged contact time, the shape changes to H4 indicating a transition from a material with open and partially blocked mesopores to a porous crystalline material [34]. By comparing pore size distributions of the material after different exposure times, explanations for the observed trend can be given. As shown in Fig. 10 after 48 h of water exposure the previously opened mesopores wider than 8 nm start to decompose with increasing length of time. This suggests an ongoing reaction of water in the wider mesopores of the material which results in a reduced pore size and pore blocking. For the present micropores and the smaller mesopores, no significant changes are visible after 6 h of exposure. Therefore, a nearly constant BET surface area despite a decreasing pore volume is received. In contrast to the storage in air, it is visible that a stronger decomposition of the sample BN-meso occurs in water. We suggest, that the decomposition of BN-ref and BN-meso are driven by their hydrophilic character. As discussed previously with water vapor adsorption, both materials possess hydrophilic regions and tend to adsorb and react with water. Thereby boron oxide and ammonia are formed, which dissolve quickly. A possible explanation for the decomposition occurring primarily in mesopores would be diffusion inhibition of the reaction products as they diffuse out of micropores. Thus, a local equilibrium is

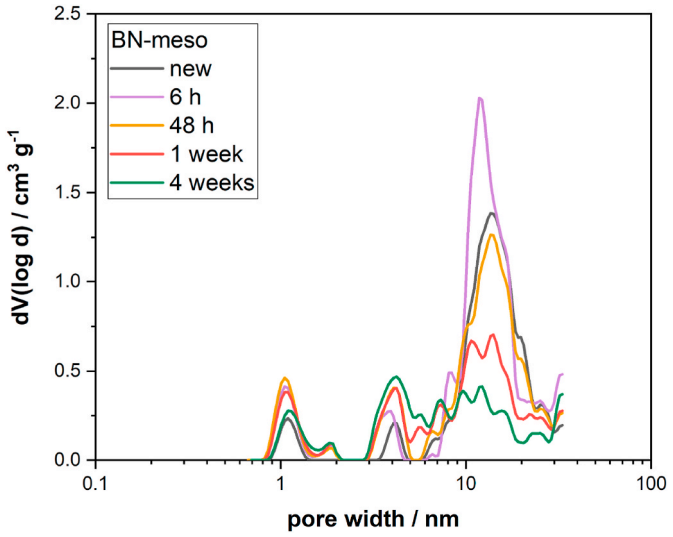

Fig. 10. Pore size distributions of BN-meso after storage in liquid water.

formed and no further reaction occurs. Another suggestion could be that the initially opened micropores are surrounded by stable crystalline BN areas and hence more water stable.

Regarding the water stability of BN-meso, it can be summarized, that larger mesopores in the material react with liquid water as well. Nevertheless, the mesoporous sample exhibits, after an initial removal of boron oxide and reaction with water, a much higher stability than BN-ref with no further changes in the BET surface area after 1 week. We expect the higher stability of BN-meso in water to arise from the higher crystallinity and thus lower amount of defect sites. If the water exposure is compared with the studies on air and vapor stability, it becomes clear that different mechanisms occur in the pore structure. While the extent of the reaction with vapor seems to depend strongly on microporosity and leads to a complete reduction of the micropore surface, the reaction with liquid water initially leads to a pore opening and thus an increase of microporosity. With prolonged contact times, wider mesopores are lost, whilst smaller mesopores and larger micropores remain constant.

4. Conclusion

In the present work, the vapor and water stability of two t-BNs with different pore structures, a micro-mesoporous sample BN-ref and a mesoporous sample BN-meso, were investigated. It was shown that the stability of t-BN is strongly related to its pore size and structure. Larger mesopores between 8 and 20 nm exhibit significantly higher stability to water vapor in air than micropores <2 nm, which was attributed to a reaction of water with the pore surface and micropore blocking. Thus, micropore surface area and micropore volume are reduced rapidly with prolonged exposure time which leads to a strong decomposition of BN-ref. On the contrary, the BN-meso showed much higher stability with an observable change in the shape of isotherms only after 12 weeks of exposure to humid air. Moreover, for the sample, no chemical decomposition was detected by XPS, XRD, or IR. Those findings were further supported by the direct adsorption of water vapor.

In addition to vapor stability, the stability of BN-ref and BN-meso to liquid water was also investigated. BN-meso exhibited higher stability to liquid water as well. However, this could not be attributed to the pore structure, since there was a visible decrease in pore volume and thus a reaction with water for both materials. Hence, the lower decomposition of BN-meso was attributed to the higher crystallinity and lesser defect sites of the initial material.

To sum up we conclude that mesoporous BN is a much more stable material for adsorption in gas phase, which may overcome current stability problems.

Author contributions

J. Hojak: Writing – original draft, Writing – review & editing, Conceptualization, Validation, Formal analysis, Investigation, Data curation, Visualization. **T. Jähnichen**: Writing – original draft, Writing – review & editing, Conceptualization, Validation, Formal analysis, Investigation, Data curation, Visualization. **Ch. Bläker**: Writing – review & editing, Supervision, Conceptualization, Project administration. **Ch. Pasel**: Writing – review & editing, Supervision, Conceptualization, Funding acquisition. **V. Mauer**: Investigation. **L. Rasmussen**: Investigation. **R. Denecke**: Writing – review & editing, Supervision. **D. Enke**: Writing – review & editing, Supervision, Conceptualization, Funding acquisition. **D. Bathen**: Writing – review & editing, Supervision, Conceptualization, Funding acquisition.

Declaration of competing interest

The authors declare that they have no known competing financial interests or personal relationships that could have appeared to influence the work reported in this paper.

Data availability

Data is available under the following adress: https://doi.org/10.17632/7nm9rfd78x.1

Acknowledgements

For their analytical support the authors would like to acknowledged S. Carstens (XRD), B. Hallack (SEM), A. Hoppe (DSC/TG), and S. Effertz (IR). For the financial support within the project BA 2012/13–1 the Institute of Technical Chemistry at the University of Leipzig and the Chair of Thermal Process Engineering at the University of Duisburg-Essen would like to thank the German Research Foundation (DFG). The publication of this article was supported by the Open Access Publication Fund of the University of Duisburg-Essen.

Appendix A. Supplementary data

Supplementary data to this article can be found online at https://doi.org/10.1016/j.rinma.2022.100338.

References

[1] T.A. Makal, J.-R. Li, W. Lu, H.-C. Zhou, Methane storage in advanced porous materials, Chem. Soc. Rev. 41 (2012) 7761–7779, https://doi.org/10.1039/C2CS35251F.
[2] J. Ortiz-Medina, Z. Wang, R. Cruz-Silva, A. Morelos-Gomez, F. Wang, X. Yao, M. Terrones, M. Endo, Defect engineering and surface functionalization of nanocarbons for metal-free catalysis, Adv. Mater. Weinheim 31 (2019), e1805717, https://doi.org/10.1002/adma.201805717.
[3] H. Huang, K. Shen, F. Chen, Y. Li, Metal–Organic frameworks as a good platform for the fabrication of single-atom catalysts, ACS Catal. 10 (2020) 6579–6586, https://doi.org/10.1021/acscatal.0c01459.
[4] P. Samanta, A.V. Desai, S. Let, S.K. Ghosh, Advanced porous materials for sensing, capture and detoxification of organic pollutants toward water remediation, ACS Sustainable Chem. Eng. 7 (2019) 7456–7478, https://doi.org/10.1021/acssuschemeng.9b00155.
[5] S. Ma, H.-C. Zhou, Gas storage in porous metal-organic frameworks for clean energy applications, Chem. Commun. 46 (2010) 44–53, https://doi.org/10.1039/B916295J.
[6] X. Gao, Y. Yao, X. Meng, Recent development on BN-based photocatalysis: a review, Mater. Sci. Semicond. 120 (2020), 105256, https://doi.org/10.1016/j.mssp.2020.105256.
[7] R. Kumar, S. Sahoo, E. Joanni, R.K. Singh, R.M. Yadav, R.K. Verma, D.P. Singh, W. K. Tan, A. Del Pérez Pino, S.A. Moshkalev, A. Matsuda, A review on synthesis of graphene, h-BN and MoS2 for energy storage applications: recent progress and perspectives, Nano Res. 12 (2019) 2655–2694, https://doi.org/10.1007/s12274-019-2467-8.
[8] J. Xiong, J. Di, W. Zhu, H. Li, Hexagonal boron nitride adsorbent: synthesis, performance tailoring and applications, J. Energy Chem. 40 (2020) 99–111, https://doi.org/10.1016/j.jechem.2019.03.002.

[9] S. Yu, X. Wang, H. Pang, R. Zhang, W. Song, D. Fu, T. Hayat, X. Wang, Boron nitride-based materials for the removal of pollutants from aqueous solutions: a review, Chem. Eng. J. 333 (2018) 343–360, https://doi.org/10.1016/j.cej.2017.09.163.
[10] I. Ihsanullah, Boron nitride-based materials for water purification: progress and outlook, Chemosphere 263 (2021), 127970, https://doi.org/10.1016/j.chemosphere.2020.127970.
[11] R. Arenal, A. Lopez-Bezanilla, Boron nitride materials: an overview from 0D to 3D (nano)structures, WIREs Comput. Mol. Sci. 5 (2015) 299–309, https://doi.org/10.1002/wcms.1219.
[12] J. Li, X. Xiao, X. Xu, J. Lin, Y. Huang, Y. Xue, P. Jin, J. Zou, C. Tang, Activated boron nitride as an effective adsorbent for metal ions and organic pollutants, Sci. Rep. 3 (2013) 3208, https://doi.org/10.1038/srep03208.
[13] J.R. Thomas, N.E. Weston, T.E. O'connor, Turbostratic1 boron nitride, thermal transformation to ordered-layer-lattice boron nitride, J. Am. Chem. Soc. 84 (1962) 4619–4622.
[14] Q. Li, L. Li, X. Yu, X. Wu, Z. Xie, X. Wang, Z. Lu, X. Zhang, Y. Huang, X. Yang, Ultrafine platinum particles anchored on porous boron nitride enabling excellent stability and activity for oxygen reduction reaction, Chem. Eng. J. 399 (2020), 125827, https://doi.org/10.1016/j.cej.2020.125827.
[15] A. Lale, S. Bernard, U.B. Demirci, Boron nitride for hydrogen storage, Chempluschem 83 (2018) 893–903, https://doi.org/10.1002/cplu.201800168.
[16] Y. Xue, P. Dai, X. Jiang, X. Wang, C. Zhang, D. Tang, Q. Weng, X. Wang, A. Pakdel, C. Tang, Y. Bando, D. Golberg, Template-free synthesis of boron nitride foam-like porous monoliths and their high-end applications in water purification, J. Mater. Chem. 4 (2016) 1469–1478, https://doi.org/10.1039/c5ta08134c.
[17] A.N. Streletskii, D.G. Permenov, B.B. Bokhonov, I.V. Kolbanev, A.V. Leonov, I. V. Berestetskaya, K.A. Streletzky, Destruction, amorphization and reactivity of nano-BN under ball milling, J. Alloys Compd. 483 (2009) 313–316, https://doi.org/10.1016/j.jallcom.2008.08.088.
[18] R. Shankar, S. Marchesini, C. Petit, Enhanced hydrolytic stability of porous boron nitride via the control of crystallinity, porosity, and chemical composition, J. Phys. Chem. C 123 (2019) 4282–4290, https://doi.org/10.1021/acs.jpcc.8b11731.
[19] S. Marchesini, X. Wang, C. Petit, Porous boron nitride materials: influence of structure, Chemistry and stability on the adsorption of organics, Front. Chem. 7 (2019) 160, https://doi.org/10.3389/fchem.2019.00160.
[20] S. Alkoy, C. Toy, T. Gönül, A. Tekin, Crystallization behavior and characterization of turbostratic boron nitride, J. Eur. Ceram. Soc. 17 (1997) 1415–1422, https://doi.org/10.1016/S0955-2219(97)00040-X.
[21] T. Jähnichen, J. Hojak, C. Bläker, C. Pasel, V. Mauer, V. Zittel, R. Denecke, D. Bathen, D. Enke, Synthesis of turbostratic boron nitride: effect of urea decomposition, ACS Omega 7 (2022) 33375–33384, https://doi.org/10.1021/acsomega.2c04003.
[22] S. Marchesini, C.M. McGilvery, J. Bailey, C. Petit, Template-free synthesis of highly porous boron nitride: insights into pore network design and impact on gas sorption, ACS Nano 11 (2017) 10003–10011, https://doi.org/10.1021/acsnano.7b04219.
[23] R. Hesse, UNIFIT 2022: Spectrum Processing, Analysis, and Presentation Software for Photoelectron Spectra (XPS), X-Ray Absorption Spectra (XAS), Auger Electron Spectra (AES) and RAMAN Spectra.
[24] C. Bläker, J. Muthmann, C. Pasel, D. Bathen, Characterization of activated carbon adsorbents – state of the art and novel approaches, ChemBioEng Reviews 6 (2019) 119–138, https://doi.org/10.1002/cben.201900008.
[25] S. Brunauer, P.H. Emmett, E. Teller, Adsorption of gases in multimolecular layers, J. Am. Chem. Soc. 60 (1938) 309–319, https://doi.org/10.1021/ja01269a023.
[26] Deutsches Institut für Normung e.V., DIN ISO 9277:2014-01, 2014th ed., Beuth Verlag GmbH, Berlin.
[27] Deutsches Institut für Normung e.V., DIN 66134:1998-02, 1998th ed., Beuth Verlag GmbH, Berlin.
[28] E.P. Barrett, L.G. Joyner, P.P. Halenda, The determination of pore volume and area distributions in porous substances. I. Computations from nitrogen isotherms, J. Am. Chem. Soc. 73 (1951) 373–380, https://doi.org/10.1021/ja01145a126.
[29] L.G. Joyner, E.P. Barrett, R. Skold, The determination of pore volume and area distributions in porous substances. II. Comparison between nitrogen isotherm and mercury porosimeter methods, J. Am. Chem. Soc. 73 (1951) 3155–3158, https://doi.org/10.1021/ja01151a046.
[30] Deutsches Institut für Normung e.V., DIN 66135:2001-06, 2001st ed., Beuth Verlag GmbH, Berlin.
[31] B. Lippens, Studies on pore systems in catalysts V. The t method, J. Catal. 4 (1965) 319–323, https://doi.org/10.1016/0021-9517(65)90307-6.
[32] R.S. Pease, An X-ray study of boron nitride, Acta Crystallogr. 5 (1952) 356–361, https://doi.org/10.1107/S0365110X52001064.
[33] M. Örnek, C. Hwang, S. Xiang, K.Y. Xie, A. Etzold, B. Yang, R.A. Haber, Effect of synthesis conditions of BCNO on the formation and structural ordering of boron nitride at high temperatures, J. Solid State Chem. 269 (2019) 212–219, https://doi.org/10.1016/j.jssc.2018.09.025.
[34] M. Thommes, K. Kaneko, A.V. Neimark, J.P. Olivier, F. Rodriguez-Reinoso, J. Rouquerol, K.S. Sing, Physisorption of gases, with special reference to the evaluation of surface area and pore size distribution (IUPAC Technical Report), Pure Appl. Chem. 87 (2015) 1051–1069, https://doi.org/10.1515/pac-2014-1117.
[35] J. Men, B. Li, J. Li, G. Li, J. Chen, X. Hou, Amorphous liquid phase induced synthesis of boron nitride nanospheres for improving sintering property of h-BN/ZrO2 composites, Ceram. Int. 46 (2020) 8031–8038, https://doi.org/10.1016/j.ceramint.2019.12.027.
[36] C.G. Cofer, J. Economy, Oxidative and hydrolytic stability of boron nitride — a new approach to improving the oxidation resistance of carbonaceous structures, Carbon 33 (1995) 389–395, https://doi.org/10.1016/0008-6223(94)00163-T.
[37] J.F. Moulder, J. Chastain (Eds.), Handbook of X-Ray Photoelectron Spectroscopy: A Reference Book of Standard Spectra for Identification and Interpretation of XPS Data, Perkin-Elmer Corporation, Eden Prairie, Minn., 1992.
[38] P.R. Kidambi, R. Blume, J. Kling, J.B. Wagner, C. Baehtz, R.S. Weatherup, R. Schloegl, B.C. Bayer, S. Hofmann, In situ observations during chemical vapor deposition of hexagonal boron nitride on polycrystalline copper, Chem. Mater. 26 (2014) 6380–6392, https://doi.org/10.1021/cm502603n.
[39] R. Geick, C.H. Perry, G. Rupprecht, Normal modes in hexagonal boron nitride, Phys. Rev. 146 (1966) 543–547, https://doi.org/10.1103/PhysRev.146.543.
[40] A. L'Hermitte, D.M. Dawson, P. Ferrer, K. Roy, G. Held, T. Tian, S.E. Ashbrook, C. Petit, Formation mechanism and porosity development in porous boron nitride, J. Phys. Chem. C 125 (2021) 27429–27439, https://doi.org/10.1021/acs.jpcc.1c08565.
[41] Q. Weng, D.G. Kvashnin, X. Wang, O. Cretu, Y. Yang, M. Zhou, C. Zhang, D.-M. Tang, P.B. Sorokin, Y. Bando, D. Golberg, Tuning of the optical, electronic, and magnetic properties of boron nitride nanosheets with oxygen doping and functionalization, Adv. Mater. Weinheim 29 (2017), https://doi.org/10.1002/adma.201700695.

DOI: 10.1016/j.rinma.2022.100338
URN: urn:nbn:de:hbz:465-20230328-112805-8